Inorg. Chem. **2008**, *47*, 6364−6374

Phosphorus Complexes of *N*-Fused Porphyrin and Its Reduced Derivatives: New Isomers of Porphyrin Stabilized via Coordination

Anna Młodzianowska, Lechosław Latos-Grażyński,* and Ludmiła Szterenberg

Department of Chemistry, University of Wrocław, 14 F. Joliot-Curie St., Wrocław 50 383, Poland

Received March 10, 2008

N-fused isophlorin **3** and its tautomeric phlorin forms **4** and **5**, the new constitutional isomers of porphyrin which preserve the basic skeleton of their maternal *N*-fused porphyrin, have been identified in the course of investigation of phosphorus insertion into *N*-fused porphyrin **2**. *N*-fused porphyrin reacts with PCl_3 in toluene yielding phosphorus(V) *N*-fused isophlorin **3**-P wherein the macrocycle acts as a trianionic tridentate ligand. The identical product has been formed in the reaction of *N*-confused porphyrin **1** and $POCl_3$ or PCl_3. The coordinating environment of phosphorus(V) in **3**-P as determined by X-ray crystallography resembles a distorted trigonal pyramid with the nitrogen atoms occupying equatorial positions with the oxygen atom lying at the unique apex. Phosphorus(V) is significantly displaced by 0.732(1) Å from the N_3 plane. The P−N distances are as follows P−N(22) 1.664(2), P−N(23) 1.645(2), and P−N(24) 1.672(2). All P−N(pyrrolic) bond lengths are markedly shorter than the P−N distances in phosphorus porphyrins. **3**-P is susceptible to proton addition at the inner C(9) carbon atom, yielding aromatic **4**-P. The modified macrocycle acts as a dianionic ligand and allows the efficient 18 π-electron delocalization pathway. Two stereoisomers affording the *syn* (**4**-P_{syn}) and *anti* (**4**-P_{anti}) location of the H(9) atom with respect to the oxygen atom of the PO unit have been identified by ^{1}H NMR. A regioselective reduction of free base *N*-fused porphyrin **2** with $NaBH_4$ yielded a nonaromatic isomer of **4**, that is, *N*-fused phlorin **5** due to an addition of a hydride to the C(15) carbon and a proton to one of the pyrrolic nitrogens. The isomer **5** reacts with PCl_3 yielding phosphorus(V) fused isophlorin **3**-P. Density functional theory has been applied to model the molecular and electronic structure of porphyrin isomers **3**, **4**, and **5** and their phosphorus(V) complexes.

Introduction

3-Halide-substituted *N*-confused porphyrin $\mathbf{1}^{Br}$ can be transformed into an 18 π-electron aromatic porphyrinoid with a fused tripentacyclic ring confined in the macrocyclic core: *N*-fused porphyrin **2**.[1,2] Mechanistically, the fused ring seems to be formed by inversion of the *N*-confused pyrrole followed by the nucleophilic attack of the adjacent pyrrole. The porphyrinoid frame is almost planar allowing an 18 π-electron aromatic conjugation which involves a peripheral route. The specific structure of **2** supports the formation of the three-centered hydrogen bonding among the pyrrolic three nitrogen atoms. *N*-fused porphyrin coordinates rhenium metal ions in a specific sitting-a-top manner.[3−5] In more general terms *N*-fused porphyrins may provide an appropriate macrocyclic setting for coordination of main group metal ions and metalloids known for their small ionic radii as already demonstrated in our studies on boron(III) *N*-fused porphyrin complexes.[6]

The phosphorus(V) ion is the smallest single ion to have been inserted into regular porphyrins.[7,8] Consequently ap-

* To whom correspondence should be addressed. E-mail: llg@wchuwr.pl.

(1) Furuta, H.; Ishizuka, T.; Osuka, A.; Ogawa, T. *J.Am. Chem. Soc.* **1999**, *121*, 2945–2946.
(2) Furuta, H.; Ishizuka, T.; Osuka, A.; Ogawa, T. *J. Am. Chem. Soc.* **2000**, *122*, 5748–5757.
(3) Toganoh, M.; Ishizuka, T.; Furuta, H. *Chem. Commun.* **2004**, 2464–2465.
(4) Toganoh, M.; Ikeda, S.; Furuta, H. *Inorg. Chem.* **2007**, *46*, 10003–10015.
(5) Toganoh, M.; Ikeda, S.; Furuta, H. *Chem. Commun.* **2005**, 4589–4591.
(6) Młodzianowska, A.; Latos-Grażyński, L.; Szterenberg, L.; Stępień, M. *Inorg. Chem.* **2007**, *46*, 6950–6957.
(7) Sanders, J. K. M.; Bampos, N.; Clyde-Watson, Z.; Darling, S. L.; Hawley, J. C.; Kim, H.-J.; Mak, C. C.; Webb, S. J. Axial Coordination Chemistry of Metalloporphyrins. In *The Porphyrin Handbook*; Kadish, K. M., Smith, K. M., Guilard, R., Eds.; Academic Press: San Diego, CA, 2000; Vol. 3, pp 1−48.
(8) Guilard, R.; van Caemelbecke, E.; Tabard, A.; Kadish, K. M. Synthesis, Spectroscopy and Electrochemical Properties of Porphyrins with Metal-Carbon. In *The Porphyrin Handbook*; Kadish, K. M., Smith, K. M., Guilard, R., Eds.; Academic Press: San Diego, CA, 2000; Vol. 3, pp 295−345.

10.1021/ic800437y CCC: $40.75
Published on Web 06/24/2008

Chart 1. *N*-Confused **1** and *N*-Fused **2** Porphyrins

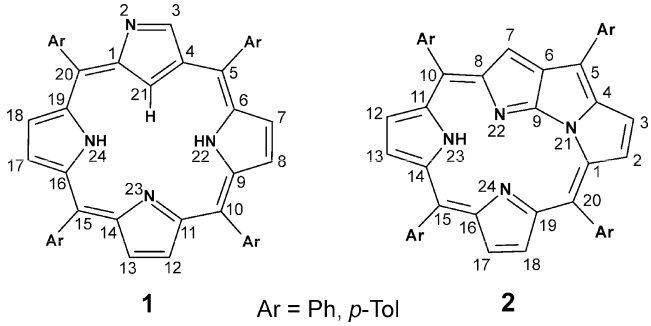

proximately octahedral phosphorus(V) porphyrin complexes are typically highly ruffled. The axial position may be occupied for a large variety of ligands of different functionality.[7–15] Such coordination of phosphorus(V) porphyrin provides a new structural motif used to create an oligomeric architecture.[11,16–19] The approach is modular in nature, and it involves simple "inorganic" reactions such as axial bond formation of a main group element, phosphorus. For instance the "wheel-and-axle-type" phosphorus(V) porphyrin oligomers, whose porphyrin rings are separated by various lengths of stable axial bridge(s) connected with the central phosphorus atoms, were explored in the elucidation of the energy and/or the electron transfer.[16–19] A porphyrin-based optical device can be constructed by applying the axial-bonding capability of a phosphorus(V) porphyrin.[11–15,20,21] Notably a reversible isomerization of two axial azobenzene subunits led to the modulation of fluorescence due to the basal tetrapyrrolic chromophore in a hexa-coordinated phosphorus(V) porphyrin, illustrating its utility as a molecular photoswitch.[12,15]

This contribution presents a new type of phosphorus(V) porphyrinoids. Originally *N*-fused porphyrin **2** has been chosen as a suitable environment for the phosphorus entrapment considering the contracted size of three nitrogen core (Chart 1).[2] Of particular importance is the observation that the phosphorus coordination stabilizes new isomers of porphyrins structurally associated with an *N*-fused porphyrin frame.

Scheme 1. Insertion of Phosphorus(V)

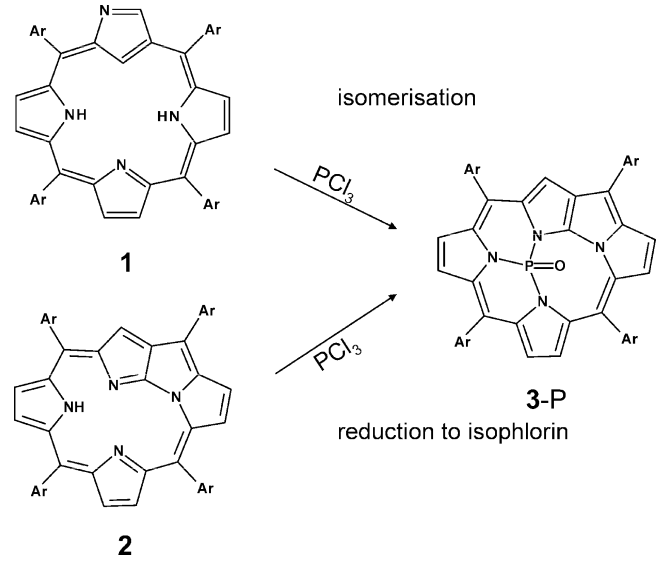

Results and Discussion

Insertion of Phophorus(V). *N*-fused porphyrin **2** reacts with PCl_3 in toluene yielding phosphorus(V) *N*-fused isophlorin **3**-P wherein the macrocycle acts as a trianionic tridentate ligand (Scheme 1).[22] Actually, the alternative pathway leads also to formation of **3**-P. Namely, our attempts to explore coordinating properties of *N*-confused porphyrin toward PCl_3 or $POCl_3$ have directly yielded **3**-P. It remains in contrast with the insertion of boron(III) to *N*-confused porphyrin as the stepwise reaction of dichlorophenylborane and **1** afforded eventually σ-phenylboron *N*-fused porphyrin in the process triggered by acid.[6]

The novel porphyrinod **3** albeit built into the **3**-P structure is structurally related to the hypothetical nonaromatic *N*-fused isophlorin (dihydro-*N*-fused porphyrin) **3** as both contain an identical macrocyclic frame.[22] In the same line of consideration, the macrocycles **2** and **3** are mutually convertible via a hydrogenation−dehydrogenation step presuming that the addition of two hydrogen atoms is localized at two internal nitrogen atoms. Such a redox relation resembles a regular porphyrin−isophlorin couple. In terms of oxidation state the *N*-fused porphyrin is two-electron oxidized with respect to porphyrin or any porphyrin isomer including directly related *N*-confused porphyrin **1**. Formally the fusion of **1** to **2** requires an extrusion of H_2. Significantly *N*-fused isophlorin **3** (Chart 2) has been identified as a nonaromatic isomer of porphyrin.

Three routes for the formation of **3**-P have been considered. Thus, the reaction of phosphrous(III) or phosphorus(V) with *N*-confused porphyrin **1** prompts the inversion of the *N*-confused pyrrole ring, followed by the fusion step allowing

(9) Brothers, P. J. *J. Porphyrins Phthalocyanines* **2002**, *6*, 259–267.
(10) Yamamoto, Y.; Akiba, K. *J. Organomet. Chem.* **2000**, *611*, 200–209.
(11) Giribabu, L.; Rao, T. A.; Maiya, B. G. *Inorg. Chem.* **1999**, *38*, 4971–4980.
(12) Reddy, D. R.; Maiya, B. G. *Chem. Commun.* **2001**, 117–118.
(13) Kiran, P. P.; Reddy, D. R.; Maiya, B. G.; Dharmadhikari, A. K.; Kumar, G. R.; Desai, N. R. *Appl. Opt.* **2002**, *41*, 7631–7636.
(14) Kumar, P. P.; Premaladha, G.; Maiya, B. G. *Chem. Commun.* **2005**, 3823–3825.
(15) Reddy, D. R.; Maiya, B. G. *J. Phys. Chem. A* **2003**, *107*, 6326–6333.
(16) Shimidzu, T.; Segawa, H. *Thin Solid Films* **1996**, *273*, 14–19.
(17) Segawa, H.; Kunimoto, K.; Susumu, K.; Taniguchi, M.; Shimidzu, T. *J. Am. Chem. Soc.* **1994**, *116*, 11193–11194.
(18) Shimidzu, T. *Synth. Met.* **1996**, *81*, 235–241.
(19) Susumu, K.; Tanaka, K.; Shimidzu, T.; Takeuchi, Y.; Segawa, H. *J. Chem. Soc., Perkin Trans.1* **1999**, 1521–1529.
(20) Kiran, P. P.; Srinivas, N. K. M. N.; Reddy, D. R.; Maiya, B. G.; Dharmadhikari, A.; Sandhu, A. S.; Kumar, G. R.; Rao, D. N. *Opt. Commun.* **2002**, *202*, 347–352.
(21) Kiran, P. P.; Reddy, D. R.; Maiya, B. G.; Rao, D. N. *Opt. Mater.* **2003**, *21*, 565–568.

(22) In this contribution we will use the terminology originally applied to regular porphyrin and its dihydrogenated derivatives (phlorin, isophlorin) to describe *N*-fused porphyrin derivatives. Thus, the hypothetical macrocycle, formed by dihydrogenation of *N*-fused porphyrin **2** localized at two internal nitrogen atoms, is named *N*-fused isophlorin **3**. Consequently, the reductions involving *meso*- or inner C(9) carbon atoms will afford *N*-fused phlorin **5** or *N*-fused inner phlorin **4**, respectively.

Chart 2. *N*-Fused Isophlorin **3**

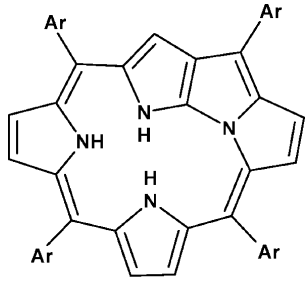

3

3-P. Albeit the appropriate mechanism remains at present unknown, the coordination of phosphorus(V) seems to be a prerequisite of the reaction sequence. Alternatively, the straightforward insertion of phosphorus(III) into *N*-fused porphyrin **2** to form **3**-P has to be correlated with an intramolecular two-electron macrocyclic reduction where the central phosphorus(III) ion acts as a two-electron reducing reagent. The third route requires an external reduction of **2** to **3** by PCl_3 which converts in the presence of water into $POCl_3$. The subsequent step involves an insertion of $POCl_3$ into the transient **3**. One can easily remove phosphorus(V) from **3**-P. The solution **3**-P was chromatographed on basic alumina recovering practically quantitatively *N*-fused porphyrin **2**. Thus, the removal of phosphorus has been accompanied by two electron oxidation of the macrocycle. Actually, the reaction of **4**(OH)-P and sodium ethoxide resulted in removal of phosphorus yielding cleanly *N*-fused porphyrin **2**.

Oxidation of **3**-P with excess of DDQ (2,3-dichloro-5,6-dicyano-*p*-benzoquinone) has immediately led to the practically quantitative formation of a phosphorus *N*-fused inner phlorin like complex **4**(OH)-P (Scheme 2). Such a reactivity seems to be general for **3**-P in the presence of oxidizing agents. For instance, the oxidation of **3**-P with dibromine or $AgBF_4$ as followed by ^1H NMR results in formation of **4**(OH)-P as well (Scheme 2). Interestingly, **4**(OH)-P underwent chlorination at the C(7) position yielding **4**$(OH)^{Cl}$-P once the solution of **4**(OH)-P had been kept at room temperature in chloroform in the presence of DDQ for four weeks (Scheme 2). At the described conditions the substitution is limited solely to the C(7) position as firmly confirmed by a ^1H NMR controlled substitution experiment. Namely, the unique H(7) singlet resonance at about 10.5 ppm has vanished because of a monosubstitution. An addition of dibromine in excess or *N*-bromosuccinimide to solution of **4**(OH)-P readily affords monobromination at C(7) yielding **4**$(OH)^{Br}$-P.

Mass spectrometry of **4**(OH)-P is consistent with the empirical formula $C_{48}H_{36}N_4O_2P$ which suggests the presence of the hydroxyl substituent in the monocationic complex **4**(OH)-P (Scheme 2). The empirical formula of **4**$(OH)^{Cl}$-P ($C_{48}H_{35}ClN_4O_2P$) has been accounted for by the presence of the hydroxyl substituent but also reveals the substitution of hydrogen by chlorine (Scheme 2). The electronic spectrum of **3**-P differs from **2** (Figure 1) which reflects the change in chromophore due to a two electron reduction.

Crystal Structure of 3-P. The molecular structure of **3**-P has been determined in X-ray investigation (Figure 2). The coordinating environment of phosphorus(V) resembles a distorted trigonal pyramid with the nitrogen atoms occupying equatorial positions with the oxygen atom lying at the unique apex.

Phosphorus(V) is significantly displaced by 0.732(1) Å from the N_3 plane (Figure 2). The P−N distances equal P−N(22) 1.664(2), P−N(23) 1.645(2), and P−N(24) 1.672(2). All P−N(pyrrolic) bond lengths are markedly shorter than the P−N distances in phosphorus(V) porphyrins which vary in the 1.801−2.054 Å range.[8,23–30] Actually the P−N bond lengths of **3**-P resemble ones determined for non macrocyclic compounds, for example, of hexamethylphosphoric triamide (1.659 and 1.649 Å).[31] The P−O bond length 1.456(1) Å approaches one determined for respective porphyrin com-

Scheme 2. Oxidation of **3**-P

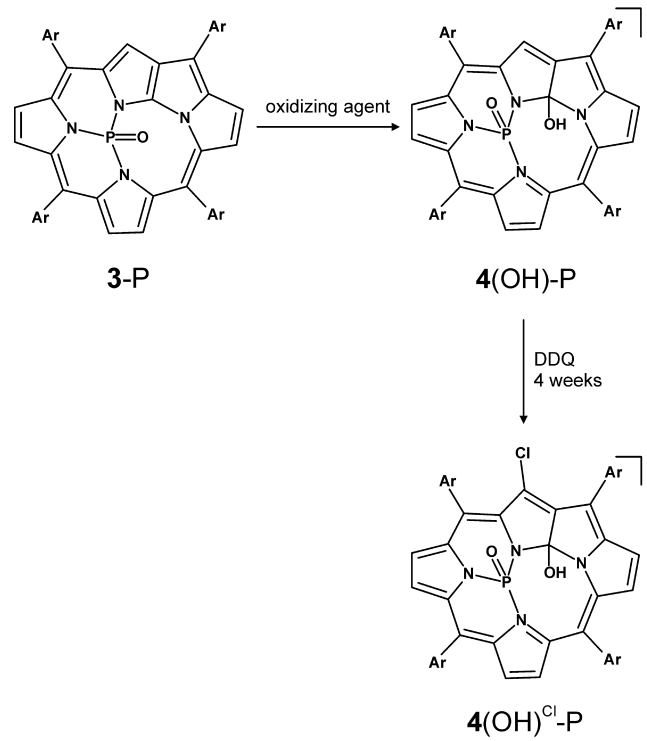

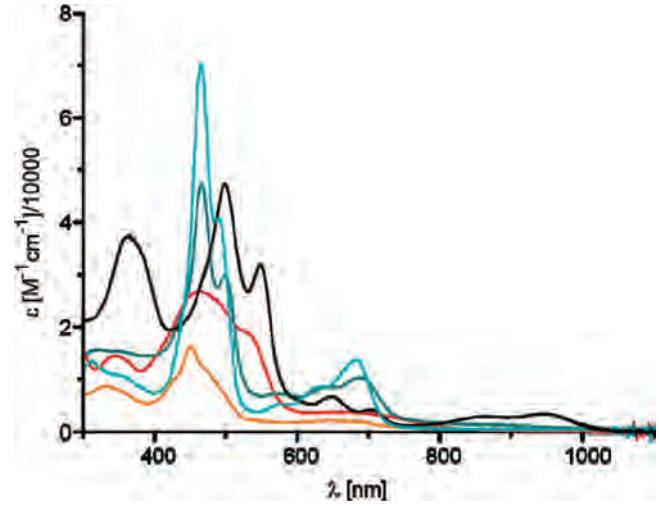

Figure 1. UV−vis spectra of **2** (black line), **3**-P (orange line), **4**(OH)-P (green line), **4**-P (blue line), and **5** (red line) in dichloromethane.

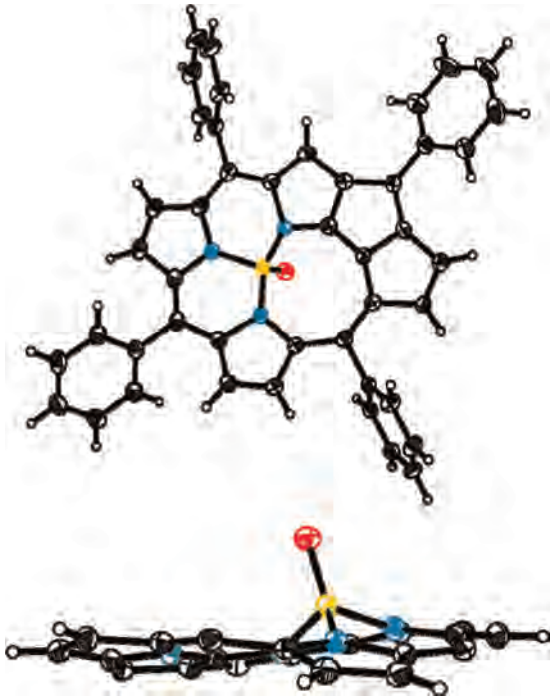

Figure 2. Molecular structure of **3**-P (top, the perspective view; bottom, the side view with phenyl groups omitted for clarity). The thermal ellipsoids represent 50% probability.

Chart 3. Canonic structures of **3**-P

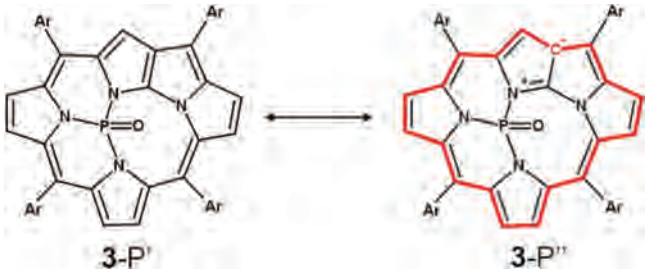

plexes which contain such a unit.[24,30] The P−O bond length of $Ph_3P{=}O$ equals 1.483 Å.[30]

The localization of double bonds within the *N*-fused isophlorin framework can be accounted for by considering the structure **3**-P′ as the major resonance contributor (Chart 3). Here the comparison to the aromatic counterparts, that is, **2**[1,2] and **2**-BPh[6] seems to be essential. Thus inspection of the bond distances determined previously for *N*-fused porphyrin[1,2] and phenylboron *N*-fused porphyrin[6] results in the conclusion that the perimeter delocalization allows the significant aromatic character. The mean deviations of bond lengths along the *N*-fused porphyrin perimeter equal 0.029 (1.363−1.458 Å) and 0.022 (1.365−1.437 Å) for *N*-fused porphyrin and its boron complex, respectively. The bond length alternation along the same perimeter of **3**-P increased noticeably as readily reflected by the mean deviation 0.042 (1.338−1.470 Å) of the bond lengths (in the calculation of mean deviations only the C−C bond lengths have been included, the limits of the bond lengths are presented in parentheses).

The dihedral angles between the macrocyclic plane and the respective phenyl rings are 10-phenyl 60.09(6)°, 15-phenyl 48.48(8)°, and 20-phenyl 66.90(6)°. These values are rather typical for 5,10,15,20-tetraarylporphyrins. In contrast, the 5-phenyl group has a tendency to coplanarity with the macrocycle as the respective dihedral angle equals 26.76(6)°. In this particular case the smaller inner angle C(4)−C(5)−C(6) 105.2(2)° has been determined. For comparison, the values of respective angles at other *meso*-positions are also given as follows C(8)−C(10)−C(11) 120.5(2)°, C(14)−C(15)−C(16) 120.7(2)°, and C(1)−C(20)−C(19) 135.4(2)°. The peculiar C(4)−C(5)−C(6) geometry is expected to be reflected by a lower activation energy of a rotation around the $C(5)_{meso}$−$C_{ipso}(5)$ allowing the overlap between the macrocyclic and phenyl π-systems. Actually, the free-base *N*-fused porphyrin[2] and its boron complex **2**-BPh[6] demonstrate the similar conformational arrangement of *meso*-aryl rings. The ^{1}H NMR studies carried out for **3**-P demonstrate clearly the influence of this structural factor on the dynamic rearrangement involving the phenyl ring rotation.

NMR Studies. The ^{1}H NMR spectrum of **4**(OH)-P (Figure 3, part B) resembles the essential features of previously reported aromatic **2**-BPh.[6] The achievable assignments of the **4**(OH)-P and **3**-P resonances, which are given above for selected groups of peaks, have been made on the basis of relative intensities and detailed two-dimensional NMR (COSY, NOESY, ROESY, HMQC, and HMBC). In particular the ^{1}H−^{31}P HMBC experiment pointed out the selected β-H hydrogens H(7), H(12), H(13), H(17), and H(18) which are coupled to a ^{31}P nucleus. In general the NMR pattern is consistent with coordination of phosphorus(V) via three nitrogen atoms. In spite of the general scaffold similarities, the spectroscopic pattern of **3**-P is markedly different from that of **4**(OH)-P as evident from the comparison of parts A and B of Figure 3. Generally, the downfield shifted perimeter resonances seen for **4**(OH)-P have been replaced by the relatively widely spread set of upfield relocated resonances assigned to **3**-P. The spectral range observed for **3**-P suggests that the macrocyclic π-delocalization pathway is essentially limited. Still, the residual paratropicity of **3**-P is evident from the peculiar features of its ^{1}H NMR spectrum. In particular, the atypical position of the H(2) resonance at 4.81 ppm has to be noted. In general, the β-H signals are shifted slightly upfield relative to their counterparts identified for nonaromatic fully conjugated systems which contain pyrrole moieties (*m*-benzipor-

(23) Mangani, S.; Meyer, E.; Cullen, D. L., Jr.; Tsutsui, M.; Carrano, C. J. *Inorg. Chem.* **1983**, *22*, 400–404.
(24) Akiba, K. Y.; Nadano, R.; Satoh, W.; Yamamoto, Y.; Nagase, S.; Ou, Z. P.; Tan, X. Y.; Kadish, K. M. *Inorg. Chem.* **2001**, *40*, 5553–5567.
(25) Cheng, P. C.; Liu, I. C.; Hong, T. N.; Chen, J. H.; Wang, S. S.; Wang, S. L.; Lin, J. C. *Polyhedron* **1996**, *15*, 2733–2740.
(26) Lin, Y. H.; Sheu, M. T.; Lin, C. C.; Chen, J. H.; Wang, S. S. *Polyhedron* **1994**, *13*, 3091–3097.
(27) Sheu, M. T.; Liu, I. C.; Cheng, P. C.; Lin, C. C.; Chen, J. H.; Wang, S. S.; Zeng, W. F. *J. Chem. Crystallogr.* **1995**, *25*, 231–235.
(28) Yamamoto, A.; Satoh, W.; Yamamoto, Y.; Akiba, K. Y. *Chem. Commun.* **1999**, 147–148.
(29) Yamamoto, Y.; Nadano, R.; Itagaki, M.; Akiba, K. *J. Am. Chem. Soc.* **1995**, *117*, 8287–8288.
(30) Yamamoto, Y.; Akiba, K. *J. Organomet. Chem.* **2000**, *611*, 200–209.
(31) Mitzel, N. W.; Lustig, C. *J. Chem. Soc., Dalton Trans.* **1999**, 3177–3183.

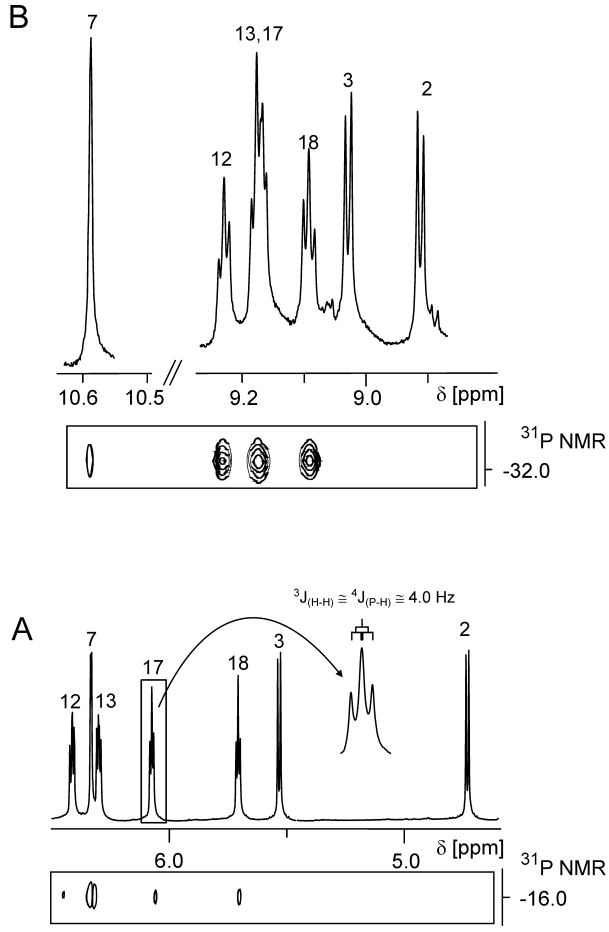

Figure 3. ^{1}H NMR spectra (A) **3**-P; (B) **4**(OH)-P (both in chloroform-*d* at 298 K). Inset in part A shows the splitting patterns of β-H resonance. The ^{1}H−^{31}P HMBC maps are shown in the bottom of each ^{1}H NMR.

phyrin, pyriporphyrin, *N*-confused pyriporphyrin, and phenolic tautomer of 22-hydroxybenziporphyrin)[32–35] including the nonaromatic isomer of porphyrin **5** discussed below.

The presence of a paratropic ring current is a commonly accepted indicator of antiaromatic character.[36] The paratropic ring current is thus a reversal of the more common diatropic current associated with aromaticity. Porphyrins and their analogues including *N*-fused porphyrin are usually aromatic in the Hückel sense, that is, the macrocycle contains a delocalization pathway containing $(4n + 2)$ π electrons. The *N*-fused porphyrin itself contains an 18 π-electron pathway and can be labeled as *N*-fused [18]porphyrin to emphasize the formal analogy with [18]annulene.[37] Porphyrin and heteroporphyrin derivatives containing $4n$ π-electron pathways, which could be expected to show antiaromatic behavior, are less common. They are normally obtained by two-electron reduction of [18]porphyrin to [20]porphyrin often known as isophlorin.[38–40] The first systems containing a [16]porphyrin ring were recently prepared by oxidation of dodecasubstituted [18]porphyrins.[41] However, these macrocycles proved nonaromatic, probably because of significant out-of-plane distortion of the macrocycle caused by bulky peripheral substitution. Interestingly, a related lithium complex [Li^{I}(TPP)][BF_4], which also contains a 16 π-electron circuit but is planar enough to show significant paratropicity.[42]

In such a context it is essential to recall 22-hydroxybenziporphyrin, a porphyrin analogue containing a phenol moiety, which has been shown to exist as an equilibrium mixture of two distinctly different tautomers.[35] One of them actually contains the hydroxyl group and shows the local [6]annulene aromaticity in the phenol fragment. The other tautomer contains a keto group and exhibits a [20]annulenoid structure characterized by macrocyclic antiaromaticity. The paratropicity of its keto form was evident from the unusual features of its ^{1}H NMR spectrum observed in the slow exchange limit. All of the signals of the peripheral β-H pyrrole protons of keto tautomer (H(9,18) 5.00, H(8,19) 5.53 H(12,13) 5.48 ppm, 203 K) are shifted upfield relative to their counterparts (H(9,18) 6.68, H(8,19) 7.38, H(12,13) 6.90 ppm) in the hydroxy tautomer.[35]

To provide a reasonable picture of the delocalization in **3**-P in terms of the classical valence bond approach, we attempted to describe the above results as a resonance hybrid of two representative canonical forms as depicted in Chart 3. The structures **3**-P′ and **3**-P″ differ substantially in the placement of formal charges and localization of double bonds. **3**-P′ with no charge separation can be expected to be the major contributor to the resonance. Still, the contributor **3**-P″ seems to be of importance as it introduces a macrocyclic conjugation allowing the [20]annulene pathway which explains the residual paratropicity.

Protonation of 3-P. An addition of an appropriate electrophile to the evidently electron rich *N*-fused macrocycle built in **3**-P has been considered as a feasible route to generate novel macrocyclic forms. Thus, a titration of **3**-P with HBF_4 in diethyl ether has been carried out in chloroform-*d* and dichloromethane-d_2 (298 K). The progress of this reaction has been systematically monitored by ^{1}H NMR. Judging by the ^{1}H NMR spectra of the reaction mixture, the process is nearly quantitative provided that there is no trace of water. In the conditions of the experiment, the protonation is not reversible.

Of particular importance is the observation that **3**-P is susceptible to protonation at C(9) yielding two stereoisomers **4**-P_{anti} and **4**-P_{syn} which are differentiated by the location of the H(9) atom with respect to the oxygen atom of the PO unit. The ^{1}H NMR spectrum of **4**-P_{anti} (Figure 4) resembles the spectrum of **4**(OH)-P and indicates the presence of a

(32) Stępień, M.; Latos-Grażyński, L. *Chem.—Eur. J.* **2001**, *7*, 5113–5117.
(33) Myśliborski, R.; Latos-Grażyński, L. *Eur. J.Org. Chem.* **2005**, 5039–5048.
(34) Myśliborski, R.; Latos-Grażyński, L. *Eur. J. Org. Chem.* **2006**, 3064–3068.
(35) Stępień, M.; Latos-Grażyński, L.; Szterenberg, L. *J. Org. Chem.* **2007**, *72*, 2259–2270.
(36) Pople, J. A.; Untch, K. G. *J. Am. Chem. Soc.* **1966**, *88*, 4811–4815.
(37) Vogel, E. *Pure Appl. Chem.* **1993**, *65*, 143–152.
(38) Cosmo, R.; Kautz, C.; Meerholtz, K.; Heinze, J.; Müllen, K. *Angew. Chem., Int. Ed. Engl.* **1989**, *28*, 604–607.
(39) Pohl, M.; Schmickler, H.; Lex, J.; Vogel, E. *Angew. Chem., Int. Ed. Engl.* **1991**, *30*, 1693–1697.
(40) Cissel, J. A.; Vaid, T. P.; Rheingold, A. L. *J. Am. Chem. Soc.* **2005**, *127*, 12212–12213.
(41) Yamamoto, Y.; Yamamoto, A.; Furuta, S.; Horie, M.; Kodama, M.; Sato, W.; Akiba, K.; Tsuzuki, S.; Uchimaru, T.; Hashizume, D.; Iwasaki, F. *J. Am. Chem. Soc.* **2005**, *127*, 14540–14541.
(42) Cissel, J. A.; Vaid, T. P.; Yap, G. P. A. *Org. Lett.* **2006**, *8*, 2401–2404.

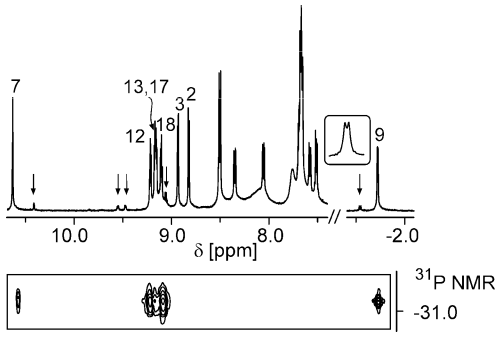

Figure 4. ^{1}H NMR spectrum of **4**-P$_{anti}$ (chloroform-*d*, 298 K). The ^{1}H−^{31}P HMBC map is shown in the bottom of the ^{1}H NMR trace. The resonances of **4**-P$_{syn}$ marked with arrows and in inset.

Scheme 3. Protonation of **3**-P

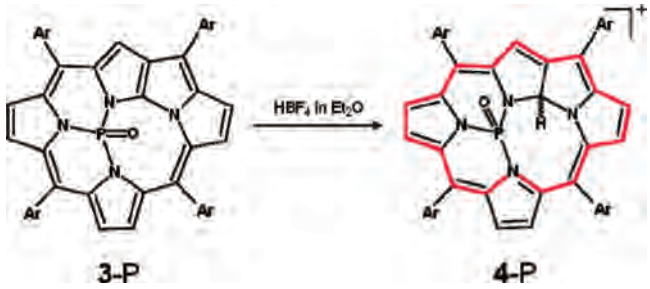

strong aromatic ring current as reflected by downfield relocation of the pyrrolic resonances. The most notable feature is the unique upfield position of the doublet assigned to H(9) resonance (−1.72 ppm, $^{3}J_{P-H(9)}$ = 3.9 Hz, chloroform-*d*, 298 K). This upfield shift is a diagnostic for substituents located in the center of the aromatic macrocycles, as found, for instance in several aromatic carbaporphyrinoids.[43–50] A new aromatic porphyrinoid *N*-fused inner phlorin **4** stabilized in **4**-P by phosphorus(V) coordination bears one hydrogen atom attached to C(9). The modified macrocycle acts as a dianionic ligand and allows the efficient 18 π-electron delocalization pathway as shown in Scheme 3. Evidently, the protonation of **3**-P at the C(9) carbon atom causes significant structural changes. For instance, the conversion of trigonal into tetrahedral geometry around C(9) is reflected by the ^{13}C NMR chemical shift of C(9) at **4**-P$_{anti}$ (65.7 ppm) which is consistent with the tetrahedral hybridization considering its substitution by two electronegative atoms. The assignment of this resonance has been unambiguously confirmed by the HMQC experiment, where correlation between C(9) and H(9) atoms has been observed.

As a matter of fact, the detailed analysis of the 0 to –5 ppm spectral region has readily resulted in the identification

(43) Chmielewski, P. J.; Latos-Grażyński, L.; Rachlewicz, K.; Głowiak, T. *Angew. Chem., Int. Ed. Engl.* **1994**, *33*, 779–781.
(44) Lash, T. D. *Angew. Chem., Int. Ed. Engl.* **1995**, *34*, 2533–2535.
(45) Hayes, M. J.; Lash, T. D. *Chem.—Eur. J.* **1998**, *4*, 508–511.
(46) Pacholska, E.; Latos-Grażyński, L.; Ciunik, Z. *Chem.—Eur. J.* **2002**, *8*, 5403–5406.
(47) Pawlicki, M.; Latos-Grażyński, L. *Chem.—Eur. J.* **2003**, *9*, 4650–4660.
(48) Stępień, M.; Latos-Grażyński, L.; Szterenberg, L.; Panek, J.; Latajka, Z. *J. Am. Chem. Soc.* **2004**, *126*, 4566–4580.
(49) Pawlicki, M.; Latos-Grażyński, L. *J. Org. Chem.* **2005**, *70*, 9123–9130.
(50) Stępień, M.; Latos-Grażyński, L.; Lash, T. D.; Szterenberg, L. *Inorg. Chem.* **2001**, *40*, 6892–6900.

Chart 4. *N*-Fused Inner Phlorin **4**

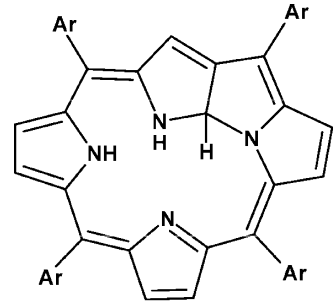

4

of the H(9) resonance assigned to a minor product formed in protonation. Namely, the intense H(9) doublet of **4**-P$_{anti}$ at −1.72 ppm is accompanied by the minor one at −1.54 ppm. The H(9) upfield position and the coupling to the coordinated ^{31}P atom allowed its unambiguous assignment. Actually, this resonance has been associated with a set of β-H pyrrolic resonances of appropriate relative intensities located at the 9−8 ppm region although strongly overlapped by the resonances of the major species. The comparison of intensities revealed that two species are formed in a 3:1 molar ratio (dichloromethane-d_2, 298 K). The available spectroscopic data are not specific for any of the two steroisomers. The Density Functional Theory (DFT) calculations demonstrated (vide infra) that the *anti* conformer is substantially more stable, and this structure has been tentatively assigned to the dominating set of resonances.

Actually a macrocyclic structural motif present at **4**-P or **4** has been previously identified.[6] Thus, the reaction of alkoxides and σ-phenylboron *N*-fused porphyrin yielded complexes where the alkoxide group has been covalently linked at the C(9) position. In more general terms, a nucleophilic attack by alkoxides on boron *N*-fused porphyrin or an electrophilic attack by proton on phosphorus(V) dihydro *N*-confused porphyrin **3**-P are applicable to create a new type of aromatic skeleton as shown schematically in Chart 4.

In fact, in our earlier studies on the reaction of dichlorophenylborane and *N*-confused porphyrin **1** we suggested initially that an insertion yielded σ-phenylboron(III) *N*-confused porphyrin where the boron(III) was expected to coordinate to two equatorial nitrogen atoms and the σ-phenyl ligand in the apical position.[6] In the course of the present studies we have recognized that the first insertion step leads to σ-phenylboron(III) *N*-fused inner phlorin **4**-BPh. The coordinating environment of boron(III) resembles a distorted trigonal pyramid with the nitrogen atoms occupying equatorial positions with the phenyl ligand lying at the unique fourth position similarly as suggested for **4**-P. The appropriate reanalysis of the NMR and DFT data (see Supporting Information) supports such a conclusion. A subsequent removal of hydride from the tertiary C(9) atom in the presence of acid afforded σ-phenylboron(III) *N*-fused porphyrin **2**-BPh.

Scheme 4. Formation of *N*-fused phlorin **5**.

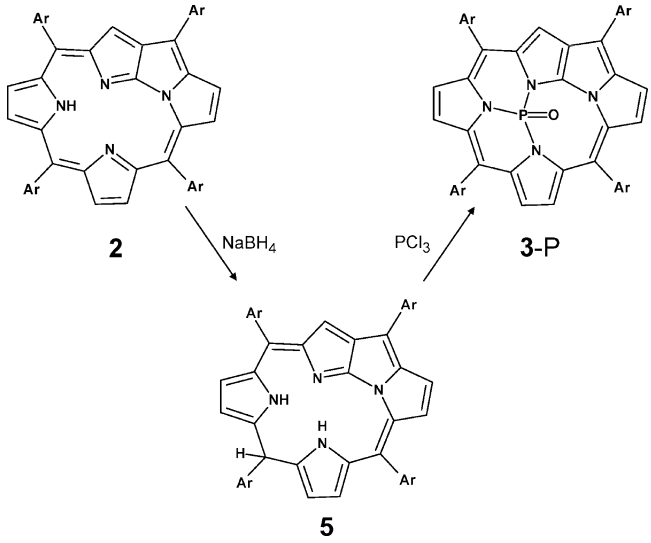

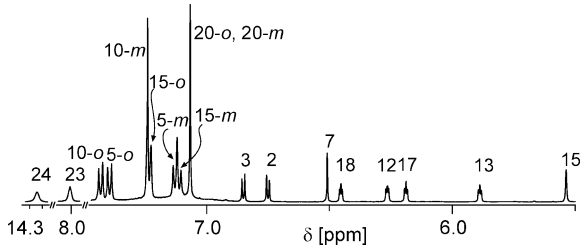

Figure 5. ^{1}H NMR spectrum of **5** (chloroform-*d*, 298 K). Peak labels follow systematic position numbering of the macrocycle or denote proton groups: *o* and *m* denote the *ortho* and *meta* positions of *meso*-*p*-tolyl rings, respectively.

Reduction of *N*-fused Porphyrin. The reduction of *N*-fused porphyrin with sodium borohydride yielded quantitatively a nonaromatic isomer of *N*-fused isophlorin, that is, *N*-fused phlorin **5** (Scheme 4).

Formally this transformation can be treated as an addition of dihydrogen to *N*-fused porphyrin. Thus, a regioselective reduction of *N*-fused porphyrin is achieved by addition of a hydride to the C(15) carbon and a proton to one of the pyrrolic nitrogens. The ^{1}H NMR spectrum of **5** is presented in Figure 5. The positions of the resonances including the NH ones reflect the structural features of **5** shown in Scheme 4.

The ^{13}C NMR chemical shift of C(15) equals 45.0 ppm and is consistent with the tetrahedral hybridization around this *meso*-carbon atom. The assignment of this resonance has been unambiguously determined by the HMQC experiment, where correlation between C(15) and H(15) atoms has been detected. The isomer **5** reacts with PCl_3 in toluene yielding phosphorus(V) *N*-fused isophlorin **3**-P.

DFT Calculations. DFT has been successfully used to describe the properties of porphyrins and related systems, providing information on their energetics, conformational behavior, tautomerism, and aromaticity.[51] We have previously applied DFT modeling to study the relationship between aromaticity, tautomerism, and coordinating capabilities of carbaporphyrinoids.[35,48,50,52–55] As determined experimentally, the specific coordination constraints of phosphorus(V) have afforded a noticeable stabilization of peculiar constitutional isomers derived form the *N*-confused porphyrin structures. These molecules have been eventually trapped as free bases or just solely as ligands being stabilized by phosphorus(V) coordination. To address the issues of the relative stabilities of porphyrin isomers **1**, **3**, **4**, and **5**, we have carried out DFT calculations performing full geometry optimization at the B3LYP/6−31G** level. Subsequently, the DFT calculations have been carried out on the selected phosphorus complexes. In each case an energy minimum was obtained. The optimized structural parameters are contained in Supporting Information, Tables S4−S13. The final geometries of the new porphyrin isomers and their complexes are shown in Figures 6–9.

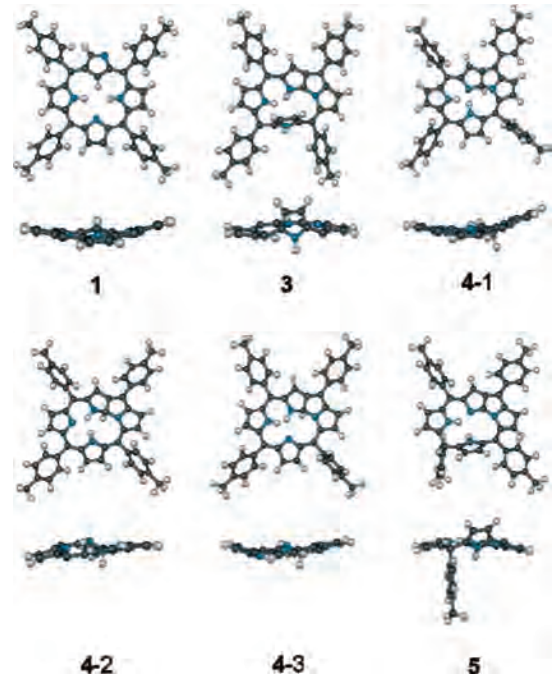

Figure 6. Geometries of *N*-confused porphyrin **1**, *N*-fused isophlorin **3**, tautomers of *N*-fused inner phlorin **4**-*n*, *N*-fused phlorin **5** as obtained in DFT optimizations (B3LYP/6−31G**). Projections emphasize the conformations of given macrocycle.

The calculated total energies, using the B3LYP/6−31G**// B3LYP/6−31G** approach, demonstrate that *N*-confused porphyrin is the most stable. Energy differences between the isomers are given in Table 1 relative to **5**. Most importantly, the isomer **5** saturated at a single *meso* position is found to be the most stable in a group of isomers derived directly from the *N*-fused porphyrin, which accounts for the experimentally detected preference for *N*-fused phlorin **5** in the solution. Thus, the relative energy of isomers increase in a series **1** < **5** < **4**-2 < **3** < **4**-1 < **4**-3. Actually these values are relatively low. An

(51) Ghosh, A. Quantum Chemical Studies of Molecular Strucutres and Potential Energy Surfaces of Porphyrins and Hemes. In *The Porphyrin Handbook*; Kadish, K. M., Smith, K. M., Guilard, R., Eds.; Academic Press: San Diego, CA, 2000; Vol. 7, pp 1−38.

(52) Myśliborski, R.; Latos-Grażyński, L.; Szterenberg, L.; Lis, T. *Angew. Chem., Int. Ed.* **2006**, *45*, 3670–3674.

(53) Pawlicki, M.; Latos-Grażyński, L.; Szterenberg, L. *Inorg. Chem.* **2005**, *44*, 9779–9786.

(54) Stępień, M.; Latos-Grażyński, L.; Szterenberg, L. *Inorg. Chem.* **2004**, *43*, 6654–6662.

(55) Pawlicki, M.; Latos-Grażyński, L.; Szterenberg, L. *J. Org. Chem.* **2002**, *67*, 5644–5653.

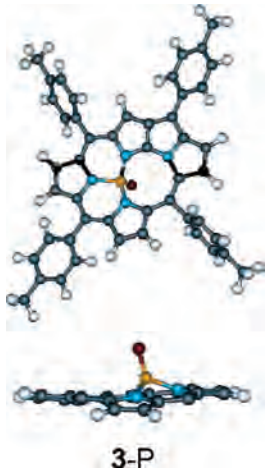

Figure 7. DFT-optimized structure of **3**-P (top, perspective view; bottom, side view). The characteristic distances and bond lengths (Å) are as follows P−N(22) 1.70, P−N(23) 1.68, P−N(24) 1.70.

Table 1. Calculated Total Energies

compound	energy [kcal/mol]
1	−15.39
3	9.40
4-1	10.55
4-2	9.34
4-3	10.93
5	0

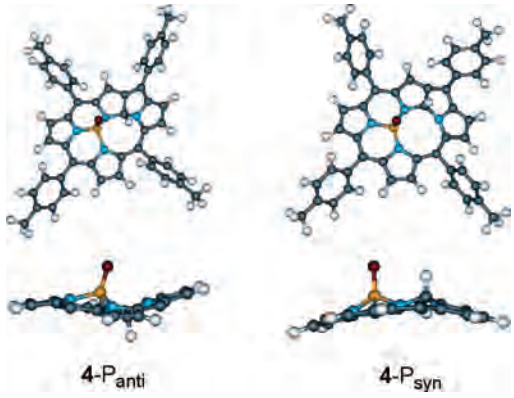

Figure 8. DFT-optimized structures of **4**-P_{anti} and **4**-P_{syn} (top, perspective view; bottom, side view). The characteristic distances and bond lengths (Å) are as follows. **4**-P_{anti}: P−N(22) 1.68, P−N(23) 1.69, P−N(24) 1.71. **4**-P_{syn}: P−N(22) 1.67, P−N(23) 1.69, P−N(24) 1.72.

analysis of the calculated relative stabilities of isomers led to the conclusion that the coordination of phosphorus may actually stabilize each isomeric structures.

Analogous DFT calculations have been carried out for representative phosphorus complexes. Originally the DFT optimization has been carried out for **3**-P using the geometry determined by X-ray crystallography as a starting point of the optimization procedure (Figure 7).

The optimized structural parameters are contained in the Supporting Information. The optimized bond lengths of **3**-P resemble those found by X-ray crystallography. The differences of the bond lengths between the DFT-optimized and crystal values are in the range of a few hundredths of angstrom.

The DFT-optimized geometries of **4**-P_{syn} and **4**-P_{anti} are shown in Figure 8. The DFT-determined P−N bond lengths of **4**-P_{syn} and **4**-P_{anti} resemble those determined by the X-ray

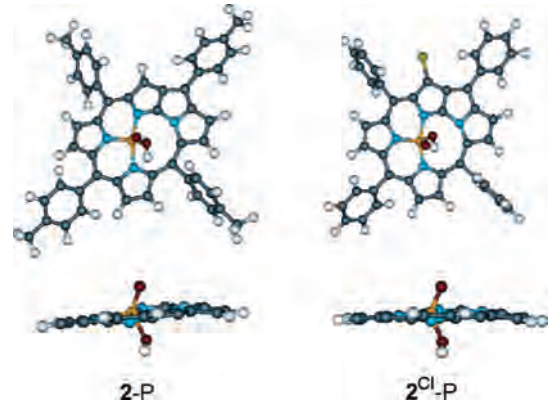

Figure 9. DFT-optimized structure of **2**-P and **2**^{Cl}-P (top, perspective view; bottom, side view). The characteristic distances and bond lengths (Å) are as follows. **2**-P: P−N(22) 1.77, P−N(23) 1.72, P−N(24) 1.76. **2**^{Cl}-P: P−N(22) 1.78, P−N(23) 1.71, P−N(24) 1.76.

study for **3**-P. However, the addition of the proton resulted in significant changes in the geometry around the C(9) carbon atom as compared to **3**-P (see Figure 8). Here the marked tendency to acquire the tetrahedral geometry is reflected by the increase of the bond lengths accompanied by the marked decrease of the N(21)−C(9)−N(22) and N(22)−C(9)−C(6) angles. However, the bond length analysis carried out for **4**-P_{syn} and **4**-P_{anti} is consistent with aromatic 18 π-electron delocalization as shown in Scheme 3. The calculated total electronic energies with zero-point energies, using the B3LYP/6−31G**//B3LYP/6−31G** approach, demonstrate that the *anti* isomer is more stable, as shown by the DFT studies, because the energy difference equals 2.75 kcal/mol.

Finally a calculation of the two electron oxidized species, which contains five coordinate phosphorus, has been carried out. The corresponding structural model of **2**-P involved the use of a fifth coordination site by a hydroxy group (an isomer of **4**(OH)-P) and is shown at Figure 9.

NICS and Chemical Shift Calculations. Nucleus-Independent Chemical Shifts (NICS) have been proposed by Schleyer et al. as a computational measure of aromaticity that is related to experimental magnetic criteria.[56,57] A NICS is defined as the negative shielding value computed at the geometric center of a ring. For monocyclic systems, NICS values generally correlate well with other established aromaticity criteria[56,57] The NICS method has been also used to assess the aromaticity of porphyrins[58,59] and their analogs.[35,60]

Here NICS values were calculated for the central 14-membered ring (center ring) of **3** and **4**-*n*. Comparison of the center ring NICS values shows that they are good indicators of macrocyclic aromaticity. For the aromatic systems **4**-*n* (**4**-1, −10.4; **4**-2, −12.6; **4**-3, −13.5) the central

(56) Schleyer, P. v. R.; Meaerker, C.; Dransfeld, A.; Jiao, H.; Hommes, N. J. R. v. E. *J. Am. Chem. Soc.* **1996**, *118*, 6317–6318.
(57) Chen, Z.; Wannere, C. S.; Corminboeuf, C.; Puchta, R.; Schleyer, P. v. R. *Chem. Rev.* **2005**, *105*, 3842–3888.
(58) Cyrański, M. K.; Krygowski, T. M.; Wisiorowski, M.; Hommes, N. J. R. v. E.; Schleyer, P. v. R. *Angew. Chem., Int. Ed. Engl.* **1998**, *37*, 177–180.
(59) Jusélius, J.; Sundholm, D. *J. Org. Chem.* **2000**, *65*, 5233–5237.
(60) Furuta, H.; Maeda, H.; Osuka, A. *J. Org. Chem.* **2001**, *66*, 8563–8572.

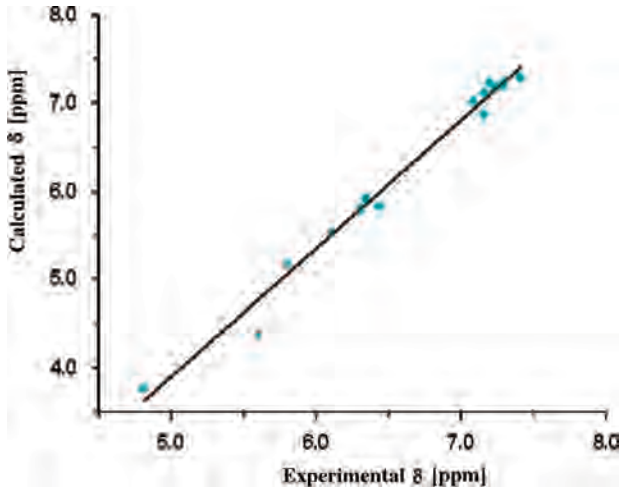

Figure 10. Linear correlation between calculated and experimental values of chemical shifts for **3**-P.

NICS values (given in parentheses) are negative and comparable with that reported for porphyrin,[58] 2-oxobenziporphyrin,[35] or dioxadiazuliporphyrin dication.[61] On the other hand for the potentially slightly antiaromatic isomer **3** the center ring NICS is still negative −2.5 indicating that the macrocyclic aromaticity is not well defined. This value is markedly smaller than the NICS obtained for [20]annulene (+12.1)[62] and is below the values calculated for the antiaromatic 22-oxybenziporphyrin (NICS, +5.0 ppm)[35] or *meso*-unsubstituted dioxadiazuliporphyrin (+4.30 ppm).[61]

^{1}H NMR chemical shifts calculated for **2**-P, **3**-P, and **4**-P using the GIAO B3LYP/6−31G** method are given in Supporting Information, Table S2. There is a very good qualitative agreement between calculated and experimental shifts, even though the diatropicity of **2**-P and **4**-P and the paratropicity of **3**-P can be exaggerated. This effect is likely due to the known propensity of the B3LYP functional to overestimate π-conjugation.[63] Nevertheless, there is a satisfactory qualitative agreement for an available set of theoretical and experimental data readily demonstrated by linear correlations between the calculated and the experimental chemical shifts as shown for the representative example of the **3**-P complex (Figure 10).

Conclusions

This study provides an insight into the coordinating properties of *N*-fused porphyrin, which can originally act as a monoanionic ligand. A preference for the coordination of small ions seems to be the inherent property of this contracted porphyrin. It is a consequence of the structural constraints imposed by an *N*-fused porphyrin structure and the presence of just three nitrogen donors in the molecular cavity. Previously we have demonstrated that *N*-fused porphyrin acts as a porphyrinoid that is capable to coordinate a single boron atom[6] which remains in contrast with a simultaneous insertion of two boron(III) ions into regular porphyrins. In this contribution we have demonstrated that *N*-fused porphyrin and porphyrinoids derived from *N*-fused porphyrin are geometrically adjusted to create a suitable coordinating center for the phosphorus(V) binding. The phosphorus(V) ion is the smallest ion to have been singularly inserted into regular porphyrins. Consequently, approximately octahedral phosphorus(V) porphyrin complexes are typically highly ruffled to afford the strained very short central ion−nitrogen bonds. The coordinating environment of phosphorus(V) *N*-fused porphyrinoids resembles a distorted trigonal pyramid where phosphorus(V) is significantly displaced from the N_3 plane and the P−N distances are markedly shorter than the P−N distances in phosphorus porphyrins.

Actually, the new molecules, applied as ligands toward phosphorus(V) reveal the peculiar plasticity of its molecular and electronic structure. The structural changes are easily triggered by two-electron reduction of *N*-fused porphyrin to yield *N*-fused isophlorin, an addition electrophilic proton at the C(9) position, or a nucleophilic hydride attack at the C(15) position. The tetrahedral−trigonal rearrangements originating at the C(9) or C(15) atom extend their consequences to the whole structure. This important feature of *N*-fused porphyrin derivatives has enabled us to investigate and eventually to control the subtle interplay between their structural flexibility and the aromaticity of the resulting forms. Of particular importance is the observation that the phosphorus coordination stabilizes new isomers of porphyrins structurally associated with an *N*-fused porphyrin frame.

All constitutional isomers of porphyrin **6** which preserve four pyrrole-related five-membered rings could be derived from regular porphyrin using straightforward strategies (Chart 5).[64,65] Thus, an approach of Vogel and co-workers involved systematic reshuffling of *meso*-carbons which lead to a family of constitutional isomers exemplified here by porphycene **7**.[37,66–68] The formal permutation of a pyrroline nitrogen and β-methine pyrrolic group affords *N*-confused (inverted) porphyrin **8**.[43,69] Finally, the formation of isoporphyrin, formally a tautomer of porphyrin with a saturated *meso*-carbon, requires relocation of the NH proton to one of *meso*-position **9**.[70,71] *N*-fused isophlorin **10** and its tautomeric forms *N*-fused inner phlorin **11** and *N*-fused phlorin **12** are constitutional isomers of porphyrin which preserve the basic

(61) Sprutta, N.; Siczek, M.; Latos-Grażyński, L.; Pawlicki, M.; Szterenberg, L.; Lis, T. *J. Org. Chem.* **2007**, *72*, 9501–9509.
(62) Castro, C.; Isborn, C. M.; Karney, W. L.; Mauksch, M.; Schleyer, P. v. R. *Org. Lett.* **2002**, *4*, 3431–3434.
(63) Wannere, C. S.; Sattelmeyer, K. W.; Schaefer, H. F., III; Schleyer, P. v. R. *Angew. Chem., Int. Ed.* **2004**, *43*, 4200–4206.
(64) Montforts, F.-P.; Glasenapp-Breiling, M.; Kusch, D. Porphyrin and Related Compounds. In *Hetarenes*; Thieme: Stuttgart; New York, 1998; pp 577−716.
(65) Sessler, J. L.; Gebauer, A.; Vogel, E. Porphyrin Isomers. In *The Porphyrin Handbook*; Kadish, K. M., Smith, K. M., Guilard, R., Eds.; Academic Press: San Diego, CA, 2000; Vol. 2, pp 1−54.
(66) Vogel, E.; Köcher, M.; Schmickler, H.; Lex, J. *Angew. Chem., Int. Ed. Engl.* **1986**, *25*, 257–259.
(67) Vogel, E.; Bröring, M.; Erben, C.; Demuth, R.; Lex, J.; Nendel, M.; Houk, K. N. *Angew. Chem., Int. Ed. Engl.* **1997**, *36*, 353–357.
(68) Wu, Y.-D.; Chan, K. W. K.; Yip, C.-P.; Vogel, E.; Plattner, D. A.; Houk, K. N. *J. Org. Chem.* **1997**, *62*, 9240–9250.
(69) Furuta, H.; Asano, T.; Ogawa, T. *J. Am. Chem. Soc.* **1994**, *116*, 767–768.
(70) Dolphin, D.; Felton, R. H.; Borg, D. C.; Fajer, J. *J. Am. Chem. Soc.* **1970**, *92*, 743–745.
(71) Barkigia, K. M.; Renner, W. M.; Xie, H.; Smith, K. M.; Fajer, J. *J. Am. Chem. Soc.* **1993**, *115*, 7894–7895.

Chart 5. Representative Constitutional Isomers of Porphyrin

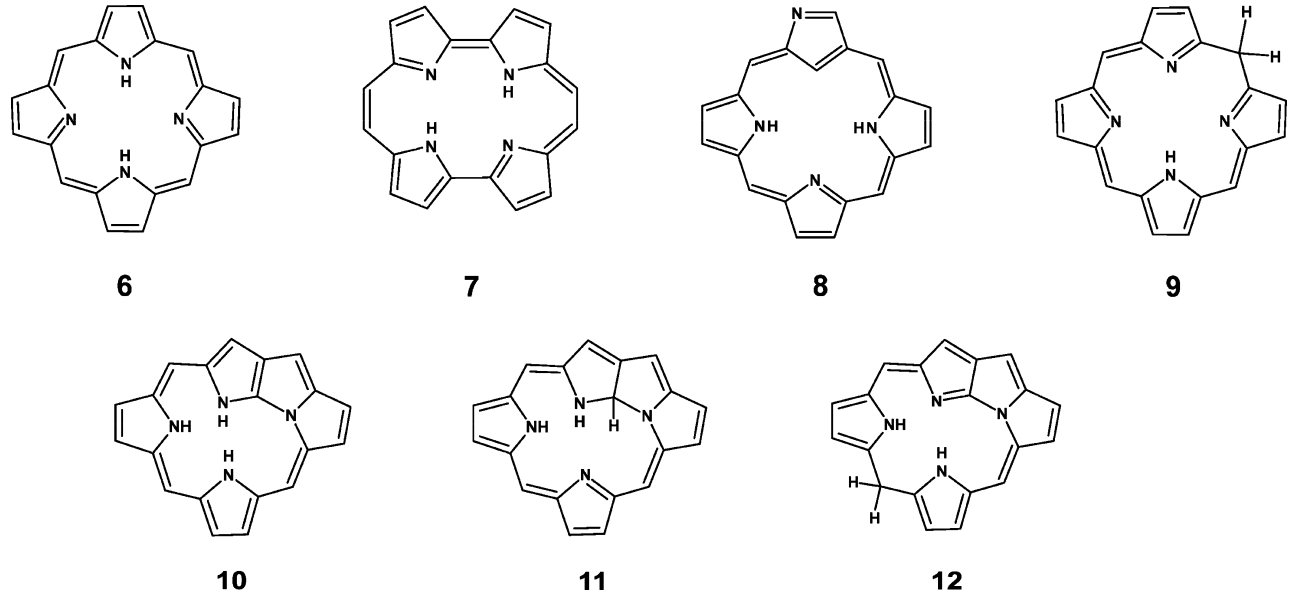

skeleton of its maternal *N*-fused porphyrin **2**.[1,2] Thus, fusion of *N*-confused porphyrin followed by reduction provides an access to a novel type of constitutional isomers of porphyrin.

Experimental Section

Materials. *N*-confused porphyrin was obtained by already described methods.[72] *N*-fused porphyrin was synthesized according the reported procedure.[2]

3-P from *N*-confused Porphyrin. A 26.8 mg quantity (0.040 mmol) of **1** was dissolved in 60 mL of toluene. Nitrogen was bubbled through the solution for 20 min. Subsequently, PCl_3 (70 μL, 0.80 mmol, 20 eq) was added. The mixture was stirred under reflux and N_2 for 74 h. The resulting mixture was evaporated to dryness with a vacuum rotary evaporator. The product was chromatographed on the silica gel column (Silicagel 40 35−70 mesh). The first orange fraction eluted with $CHCl_3$ stabilized by amylene contained the desired product. The solvent was evaporated, and the brown solid **3**-P was dried in vacuum. Yield 14.3 mg, 50%.

3-P from *N*-fused Porphyrin. A 9.6 mg quantity (0.014 mmol) of **2** was dissolved in 60 mL of toluene. Nitrogen was bubbled through the solution for 20 min. Subsequently, PCl_3 (25 μL, 0.29 mmol, 20 eq) was added. The mixture was stirred under reflux and N_2 for 65 h. The resulting mixture was evaporated to dryness with a vacuum rotary evaporator. The product was chromatographed on the silica gel column (Silicagel 40 35−70 mesh). The first orange fraction eluted with $CHCl_3$ stabilized by amylene contained the desired product. The solvent was evaporated, and the brown solid **3**-P was dried in vacuum. Yield 9 mg, 59.0%.

3-P from *N*-fused Phlorin. A 4.2 mg quantity (0.0063 mmol) of **5** was dissolved in 40 mL of toluene. Nitrogen was bubbled through the solution for 20 min. Subsequently, PCl_3 (11 μL, 0.125 mmol, 20 eq) was added. The mixture was stirred under reflux and N_2 for 65 h. The resulting mixture was evaporated to dryness with a vacuum rotary evaporator. The product was chromatographed on the silica gel column (Silicagel 40 35−70 mesh). The first orange fraction eluted with $CHCl_3$ stabilized by amylene contained the desired product. The solvent was evaporated, and the brown solid **3**-P was dried in vacuum. Yield 1.6 mg, 35.5%.

^{1}H NMR (500 MHz, CD_2Cl_2, 298 K): δ = 7.41 (2H, $^3J_{(H,H)}$ = 7.8 Hz, 10-*o*), 7.29 (2H, $^3J_{(H,H)}$ = 8.3 Hz, 10-*m*), 7.29 (2H, $^3J_{(H,H)}$ = 8.0 Hz, 15-*o*), 7.23 (2H, $^3J_{(H,H)}$ = 7.8 Hz, 15-*m*), 7.20 (2H, $^3J_{(H,H)}$ = 8.0 Hz, 20-*o*), 7.16 (4H, $^3J_{(H,H)}$ = 7.6 Hz, 5-*o*, 20-*m*), 7.08 (2H, $^3J_{(H,H)}$ = 8.0 Hz, 5-*m*), 6.43 (dd, 1H, $^3J_{(H,H)} \cong$ 5 Hz, $^4J_{(H,P)} \cong$ 5 Hz, H12), 6.34 (1H, $^4J_{(H,P)}$ = 2.3 Hz, H7), 6.31 (dd, 1H, $^3J_{(H,H)} \cong$ 4 Hz, $^4J_{(H,P)} \cong$ 4 Hz, H13), 6.10 (br., 1H, H17), 5.80 (∼t, 1H, $^3J_{(H,H)} \cong$ 4 Hz, $^4J_{(H,P)} \cong$ 4 Hz, H18), 5.60 (AB, 1H, $^3J_{(H,H)}$ = 5.5 Hz, H3), 4.81 (AB, 1H, $^3J_{(H,H)}$ = 6.0 Hz, H2), 2.43 (s, 3H, 10-Me), 2.38 (s, 6H, 15-Me, 20-Me), 2.29 ppm (s, 3H, 5-Me). ^{13}C NMR (125.7 MHz, $CDCl_3$, 298 K): δ = 148.9, 142.4, 142.4, 139.3, 138.1, 137.8, 137.0, 136.2, 136.2, 136.1, 135.6, 135.2, 135.2, 134.6, 134.5, 131.9, 131.4, 131.2, 130.7, 130.4, 130.2, 130.1, 129.4, 129.3, 129.2, 129.1, 128.1, 126.5, 126.4, 126.0, 123.6, 123.6, 123.0, 122.9, 122.6, 114.8, 113.8, 113.7, 113.7, 113.0, 108.3, 108.3, 108.1, 108.1, 21.3, 21.3, 21.2, 21.2 ppm. ^{31}P NMR (202.4 MHz, $CDCl_3$, 298 K) −16.9 ppm. UV−vis (CH_2Cl_2) λ_{max} (log ε) = 332 (3.94), 450 (4.21), 667 nm (3.29). HRMS (ESI, *m*/*z*): 714.2545 (calcd 714.2548 for $[C_{48}H_{35}N_4OP]$ (M)).

4(OH)-P. $AgBF_4$ in excess was added to the dichloromethane solution of **3**-P (5.7 mg, 0.0080 mmol). When the color changed from orange to green-brown, the solid impurities were removed by filtration and the solution was evaporated to dryness. The crude product was recrystallized from CH_2Cl_2/hexane. Yield 2.7 mg, 46.1%.

^{1}H NMR (500 MHz, $CDCl_3$, 298 K): δ = 10.60 (s, 1H, H7), 9.23 (∼t, 1H, $^3J_{(H,H)} \cong$ 4 Hz, $^4J_{(H,P)} \cong$ 4 Hz, H12), 9.18 (m, 2H, H13, H17), 9.09 (∼t, 1H, $^3J_{(H,H)} \cong$ 5 Hz, $^4J_{(H,P)} \cong$ 5 Hz, H18), 9.03 (AB, 1H, $^3J_{(H,H)}$ = 4.8 Hz, H3), 8.92 (AB, 1H, $^3J_{(H,H)}$ = 4.8 Hz, H2), 8.56 (2H, $^3J_{(H,H)}$ = 8.0 Hz, 5-*o*), 8.20 (1H, $^3J_{(H,H)}$ = 8.7 Hz, 20-*o*), 8.12 (1H, $^3J_{(H,H)}$ = 8.9 Hz, 20-*o*), 8.10 (1H, $^3J_{(H,H)}$ = 8.0 Hz, 15-*o*), 7.67 (m, 4H, 15-*m*, 5-*m*), 7.63 (2H, $^3J_{(H,H)}$ = 8.0 Hz, 20-*m*), 2.74 (s, 3H, 20-Me), 2.70 (s, 3H, 10/15-Me), 2.69 (s, 3H, 15/10-Me), 2.59 ppm (s, 3H, 5-Me). ^{31}P NMR (202.4 MHz, CD_2Cl_2, 298 K) −32.3 ppm. UV−vis (CH_2Cl_2) λ_{max} (log ε) = 318 (4.19), 349 (4.19), 466 (4.68), 498 (4.47), 572 (3.86), 641 (3.93), 688 nm (4.01). HRMS (ESI, *m*/*z*): 731.2650 (calcd 731.2576 for $[C_{48}H_{36}N_4O_2P]^+$ (M^+)).

4-P. Phosphorus *N*-fused inner phlorin **4**-P has been generated by addition of HBF_4 in Et_2O to **3**-P. An HBF_4 titration has been carried out in chloroform-*d* in anaerobic conditions, and the progress of this reaction has been monitored by ^{1}H NMR. The solution of

$HBF_4$was gradually added using a microsyringe. The solution color changed from orange to green in the course of titration. Typically the conversion is quantitative.

^{1}H NMR (500 MHz, $CDCl_3$, 213 K): δ = 10.76 (br, 1H, H7), 9.29 (br, 1H, H12), 9.26 (br, 1H, H13), 9.21 (br, 1H, H17), 9.11 (br, 1H, H18), 8.98 (AB, 1H, $^3J_{(H,H)}$ = 3.9 Hz, H3), 8.83 (AB, 1H, $^3J_{(H,H)}$ = 3.9 Hz, H2), 8.68 (1H, $^3J_{(H,H)}$ = 5.7 Hz, 10-*o*), 8.49 (2H, $^3J_{(H,H)}$ = 6.7 Hz, 5-*o*), 8.28 (2H, $^3J_{(H,H)}$ = 6.4 Hz, 15-*o*, 20-*o*), 8.09 (s, 1H, $^3J_{(H,H)}$ = 7.6 Hz, 20-*o*), 8.07 (1H, $^3J_{(H,H)}$ = 7.6 Hz, 10-*o*), 7.92 (1H, $^3J_{(H,H)}$ = 6.7 Hz, 15-*o*), 7.87 (1H, $^3J_{(H,H)}$ = 6.9 Hz, 10-*m*), 7.71 (m, 2H, 15-*m*), 7.66 (m, 4H, 5-*m*, 20-*m*), 7.58 (m, 1H, 10-*m*), 2.71 (s, 3H, 10-Me), 2.69 (s, 3H, 20-Me), 2.68 (s, 3H, 15-Me), 2.58 (s, 3H, 5-Me), −1.74 ppm (s, 1H, H9). ^{13}C NMR (125.7 MHz, $CDCl_3$, 298 K): δ = 158.2, 152.1, 144.0, 142.3, 140.9, 140.6, 140.0, 139.9, 139.6, 139.5, 137.0, 137.0, 136.0, 135.9, 135.6, 134.3, 134.1, 133.5, 132.4, 132.0, 131.8, 131.3, 130.9, 130.3, 129.8, 128.8, 128.6, 127.9, 127.6, 127.6, 127.1, 126.9, 126.0, 125.0, 124.9, 118.7, 118.5, 117.1, 115.8, 65.7(C9), 21.6, 21.6, 21.5 ppm. ^{31}P NMR (202.4 MHz, $CDCl_3$, 298 K) –31.4 ppm. UV−vis (CH_2Cl_2) λ_{max} (log ε) = 312 (4.13), 465 (4.85), 491 (4.61), 576 (3.71), 629 (3.93), 684 nm (4.13). HRMS (ESI, *m*/*z*): 715.2561 (calcd 715.2626 for $[C_{48}H_{36}N_4OP]^+$ $[M^+]$).

5. *N*-fused porphyrin **2** (5.5 mg) was dissolved in THF, and 31.1 mg of $NaBH_4$ was added. The mixtures was stirred at room temperature overnight. The solid deposit was removed by filtration, and the solution was evaporated to dryness. The crude product was recrystallized from CH_2Cl_2/hexane. Yield 4.7 mg, 85.4%.

^{1}H NMR (500 MHz, $CDCl_3$, 298 K): δ = 14.27 (s, 1H, H24), 8.00 (s, 1H, H23), 7.43 (2H, $^3J_{(H,H)}$ = 8.0 Hz, 10-*o*), 7.40 (2H, $^3J_{(H,H)}$ = 8.0 Hz, 5-*o*), 7.28 (4H, $^3J_{(H,H)}$ = 6.9 Hz, 10-*m*, 15-*o*), 7.12 (2H, $^3J_{(H,H)}$ = 8.0 Hz, 5-*m*), 7.11 (2H, $^3J_{(H,H)}$ = 7.8 Hz, 15-*m*), 7.07 (s, 4H, 20-*o*, 20-*m*), 6.85 (AB, 1H, $^3J_{(H,H)}$ = 5.7 Hz, H3), 6.75 (AB, 1H, $^3J_{(H,H)}$ = 5.5 Hz, H2), 6.51 (s, 1H, H7), 6.45 (∼t, 1H, $^3J_{(H,H)} \cong$ 3 Hz, $^4J_{(H,H)} \cong$ 3 Hz, H18), 6.26 (dd, 1H, $^3J_{(H,H)}$ = 3.6 Hz, $^4J_{(H,H)}$ = 2.3 Hz, H12), 6.19 (∼t, 1H, $^3J_{(H,H)} \cong$ 3 Hz, $^4J_{(H,H)} \cong$ 3 Hz, H17), 5.89 (∼t, 1H, $^3J_{(H,H)} \cong$ 3 Hz, $^4J_{(H,H)} \cong$ 3 Hz, H13), 5.54 (s, 1H, H15), 2.43 (s, 3H, 10-Me), 2.32 (s, 6H, 5 and 20-Me), 2.31 (s, 3H, 15-Me). ^{13}C NMR (125.7 MHz, $CDCl_3$, 298 K): δ = 160.8, 151.3, 151.1, 142.2, 139.2, 138.7, 137.6, 137.3, 137.2, 137.1, 136.8, 136.1, 136.0, 134.2, 134.1, 133.9, 131.3, 131.2, 131.2, 131.0, 130.0, 129.4, 129.4, 129.0, 128.6, 125.9, 122.4, 120.4, 119.7, 115.2, 113.7, 109.8, 108.9, 45.0(C15), 21.4, 21.1, 21.2, 21.1 ppm. UV−vis (CH_2Cl_2) λ_{max} (log ε) = 343 (4.16), 459 (4.43), 677 nm (3.56). HRMS (ESI, *m*/*z*): 671.3148 (calcd 671.3174 for $[C_{48}H_{39}N_4]^+$ ($[M + H]^+$)).

DFT Calculations. DFT calculations were performed with the GAUSSIAN03 program.[73] Geometry optimizations were carried out within unconstrained C_1 symmetry, with starting coordinates derived from X-ray structural data. Becke's three-parameter exchange functionals[74] with the gradient-corrected correlation formula of Lee, Yang, and Parr (DFT(B3LYP))[75] were used with the 6−31G** basis set.[76] Harmonic vibrational frequencies were calculated using analytical second derivatives. Structures were found to have converged to a minimum on the potential energy surface.

Instrumentation. NMR spectra were recorded on a Bruker Avance 500 spectrometer. UV−vis electronic spectra were recorded on a diode array Hewlett-Packard 8453 spectrometer and Varian Cary 50 Bio. Mass spectra were recorded on a Bruker micrOTOF-Q spectrometer using the electrospray and liquid matrix secondary-ion mass spectrometry techniques.

X-Ray Analysis. X-ray quality crystals of **3**-P were prepared by diffusion of hexane into dichloromethane/chloroform-*d* solution contained in a thin tube. Data were collected at 100 K on an Xcalibur PX kappa-geometry diffractometer with CCD Onyx camera. The data were corrected for Lorentz and polarization effects. Crystal data are compiled in Supporting Information, Table S1. The structure was solved by direct methods with SHELXS-97 and refined by the full-matrix least-squares method by using SHELXL-97 with anisotropic thermal parameters for the non-hydrogen atoms. Scattering factors were those incorporated in SHELXS-97.[77,78]

Acknowledgment. Financial support from the Ministry of Science and Higher Education (Grant PBZ-KBN-118/T09/2004) is kindly acknowledged. Quantum chemical calculations have been carried out at the Poznań Supercomputer Center (Poznań).

Supporting Information Available: Tables of computational results (Cartesian coordinates, tables) and additional NMR data are included (PDF). This material is available free of charge via the Internet at http://pubs.acs.org.

IC800437Y

(72) Geier, G. R., III; Haynes, D. M.; Lindsey, S. *Org. Lett.* **1999**, *1*, 1455–1458.
(73) Frisch, M. J.; Trucks, G. W.; Schlegel, H. B.; Scuseria, G. E.; Robb, M. A.; Cheeseman, J. R.; Montgomery, J. A., Jr.; Vreven, T.; Kudin, K. N.; Burant, J. C.; Millam, J. M.; Iyengar, S. S.; Tomasi, J.; Barone, V.; Mennucci, B.; Cossi, M.; Scalmani, G.; Rega, N.; Petersson, G. A.; Nakatsuji, H.; Hada, M.; Ehara, M.; Toyota, K.; Fukuda, R.; Hasegawa, J.; Ishida, M.; Nakajima, T.; Honda, Y.; Kitao, O.; Nakai, H.; Klene, M.; Li, X.; Knox, J. E.; Hratchian, H. P.; Cross, J. B.; Adamo, C.; Jaramillo, J.; Gomperts, R.; Stratmann, R. E.; Yazyev, O.; Austin, A. J.; Cammi, R.; Pomelli, C.; Ochterski, J. W.; Ayala, P. Y.; Morokuma, K.; Voth, G. A.; Salvador, P.; Dannenberg, J. J.; Zakrzewski, V. G.; Dapprich, S.; Daniels, A. D.; Strain, M. C.; Farkas, O.; Malick, D. K.; Rabuck, A. D.; Raghavachari, K.; Foresman, J. B.; Ortiz, J. V.; Cui, Q.; Baboul, A. G.; Clifford, S.; Cioslowski, J.; Stefanov, B. B.; Liu, G.; Liashenko, A.; Piskorz, P.; Komaromi, I.; Martin, R. L.; Fox, D. J.; Keith, T.; Al-Laham, M. A.; Peng, C. Y.; Nanayakkara, A.; Challacombe, M.; Gill, P. M. W.; Johnson, B.; Chen, W.; Wong, M. W.; Gonzalez, C.; Pople, J. A. *Gaussian 03*, Revision C.01; Pittsburgh, PA, **2004**.
(74) Becke, A. D. *Phys. Rev. A* **1988**, *38*, 3098–3100.
(75) Lee, C.; Yang, W.; Parr, R. G. *Phys. Rev. B* **1988**, *37*, 785–789.
(76) Hay, P. J.; Wadt, W. R. *J. Chem. Phys.* **1985**, *82*, 270–283, 284−298, 299−310.
(77) Sheldrick, G. M. *SHELXS97, program for solution of crystal structures*; University of Göttingen: Göttingen, Germany, 1997.
(78) Sheldrick, G. M. *SHELXL97, program for crystal structure refinement*; University of Göttingen: Göttingen, Germany, 1997.